Phase Relations and the Effects of Ordering in $Zn_{2x}(AgIn)_yMn_{2z}Te_2$ Alloys

Rafael Tovar and Miguel Quintero

Centro de Estudios de Semiconductores, Departamento de Física, Universidad de Los Andes, Mérida, Venezuela

Champa Neal and John C. Woolley

Ottawa-Carleton Institute for Physics, University of Ottawa, Ottawa, Ontario, Canada K1N 6N5

ABSTRACT

The T *vs.* composition phase diagram of the alloy system $Zn_{2x}(AgIn)_yMn_{2z}Te_2$ ($x + y + z = 1$) was investigated in the range $0 < z < 0.7$ by differential thermal analysis and x-ray diffraction measurements. Samples were prepared for various lines of constant x/y ratio and the $T(z)$ data determined for each line. Values of lattice parameters were determined for all samples and the limits of single-phase solid solution estimated. In addition to liquidus and solidus curves, the zinc-blende → chalcopyrite and Mn-disordered → Mn-ordered transition lines were determined, these phase fields being the ones of interest in the measurements of optical energy gap and of magnetic properties.

Most of the work (1, 2) on semimagnetic semiconductor alloys has been concerned with alloys of the form $II_{1-z}Mn_zVI$. However, similar alloys can be produced from the chalcopyrite $I.III.VI_2$ compounds, the ternary analogs of the II VI compounds. The crystallographic and optical energy gap values of a number of alloy systems of the form $(I\ III)_{1-z})Mn_{2z}Te_2$ have been investigated (3-7), and also the work has been extended to the more general $Cd_{2x}(I.III)_{1-z}Mn_{2z}Te_2$ alloys (8, 9).

These chalcopyrite-based alloys are of interest because, depending upon the heat-treatment, the alloys can be produced with the Mn atoms either at random or ordered (or partially ordered) on the cation sublattice. The optical energy gap values and the magnetic behavior are very different in the two different conditions (7-10). Before a detailed investigation of the effects of this ordering can be carried out, it is necessary to choose the heat-treatment of the alloys so as to produce the required ordered or disordered condition. For this purpose, a detailed knowledge of the T *vs.* composition phase diagram is required. Most of the work so far has been concerned with the Cd-base alloys [*e.g.*, (3, 4)], with little work on Zn-based materials. Garbato and Ledda (11) investigated the crystallography of the $Zn_{2x}(CuIn)_{1-x}Te_2$ alloys, and recently the present authors have given the crystallography and optical energy gap values of the $Zn_{2x}(CuIn)_yMn_{2z}Te_2$ and $Zn_{2x}(AgIn)_yMn_{2z}Te_2$ alloys (12). In the present work, this investigation of the Zn-based alloys has been extended to the study of the $T(z)$ diagrams of various sections of the alloy system $Zn_{2x}(AgIn)_yMn_{2z}Te_2$ ($x + y + z = 1$).

Preparation of Samples and Experimental Measurements

All of the alloys used were produced by the usual melt and anneal technique (12, 13). The components of each 1.5g sample were sealed under vacuum in small quartz ampuls, which had previously been carbonized to prevent interaction of the alloy with the quartz, and heated to 1150°C. This temperature is lower than the melting temperature of manganese, which will, however, dissolve in the liquid

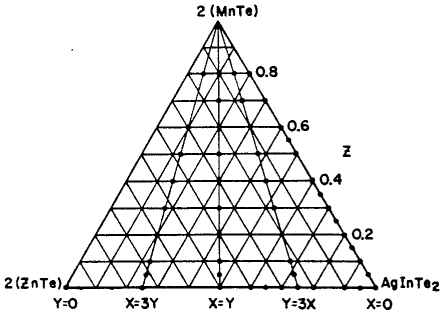

Fig. 1. Composition diagram for the $Zn_{2x}(AgIn)_yMn_{2z}Te_2$ alloys. ● Composition of alloys used in the present work.

components and some of the resultant phases. The resulting alloy must be annealed to equilibrium at a lower temperature. As in all such multicomponent alloys, the appropriate temperature of anneal is not easily determined until the T *vs.* composition phase diagram is known for each section. However, the results for the sections $(AgIn)_{1-z}Mn_{2z}Te_2$ and $Zn_{2x}(AgIn)_{1-x}Te_2$ already investigated (6, 13) show that an annealing temperature of 600°C should be satisfactory, and this value was used here. It has been found that at least 20-30 days of annealing is necessary to obtain equilibrium conditions at 600°C, since as indicated above, long-range diffusion may be required after the initial cooling from 1150°C. Equilibrium at fairly low temperature is needed if peaks corresponding to order-disorder and chalcopyrite-zinc-blende transitions are to be observed in the heating DTA runs. However, once equilibrium at 600°C has been achieved, the zinc-blende-chalcopyrite and order-disorder transitions, which involve only short-range diffusion, can occur in much shorter times, even though they occur below 600°C in these systems. In order to produce useful $T(z)$ diagrams, samples were prepared for the sections given by $x = 3y$, $x = y$, $y = 3x$, $x = 0$, and $z = 0$, as shown in Fig. 1. Since the interest of the program is in semimagnetic semiconductors, values of z up to an upper limit of 0.7 were used, and larger values of z were not investigated.

X-ray powder photographs, either Guinier or Debye-Scherrer, were used to check the condition of the annealed samples and to determine the phases that were present. Values of the lattice parameter were determined for the zinc blende and chalcopyrite phases, these results having been reported previously (12).

Phase transition temperatures were obtained from DTA measurements (14) using a closed-tube configuration and with silver or gold used as the reference material. The charge was a powdered alloy of approximately 100 mg weight. The temperatures of the sample and of the reference were measured with Chromel-Alumel thermocouples, the difference signal between sample and reference and also the temperature signal being simultaneously registered on a two-pen chart recorder. Each phase transition temperature was determined from the base-line intercept of the tangent to the leading edge of the peak in the difference signal. Both heating and cooling runs were made for each sample. The heating rate was such that the system went from room temperature to 1150°C in approximately 1.5-2h. Cooling was carried out by switching off the power to the furnace and the resulting cooling rate was slower than the heating rate. Peaks in the difference curve could be detected down to about 1 μV, below which value they could not be distinguished from background noise, etc. The accuracy of the peak temperatures has been estimated as ±15°C.

Results and Discussion

In previous work in the $Zn_{2x}(AgIn)_yMn_{2z}Te_2$ alloys (12), lattice parameter values for samples slowly cooled to room temperature were used to determine the composition ranges of the various single-phase fields involving the zinc blende and chalcopyrite phases. With regard to the T *vs.* composition data, the $T(z)$ diagram for the $(AgIn)_{1-z}Mn_{2z}Te_2$ section, *i.e.*, $x = 0$, was given previously (6), and recently the $T(x)$ diagram has been obtained for the $Zn_{2x}(AgIn)_{1-x}Te_2$ section (13), *i.e.*, $z = 0$. For comparison purposes, these two diagrams are shown in Fig. 3 and 2, respectively. For the case of the $Zn_{1-z}Mn_zTe$ section, *i.e.*, $y = 0$, no data seem to be available.

The $T(z)$ diagrams for the sections $y = 3x$, $x = y$, and $x = 3y$ are shown in Fig. 4, 5, and 6, respectively. In these diagrams, boundaries determined directly from DTA measurements are shown as solid lines. However, some boundaries cannot be determined from the DTA data and these need to be estimated from the lattice parameter and energy gap values determined previously (12). These boundaries are shown as dash-dotted lines in the $T(z)$ diagrams while dashed lines have been used to indicate lines which are estimates only. The range of the present experimental results is from room temperature to 1200°C. Hence, since the melting point of ZnTe is 1290°C (11), for the present alloys it was not possible to obtain values for the liquidus curves except for a small range of composition close to $AgInTe_2$.

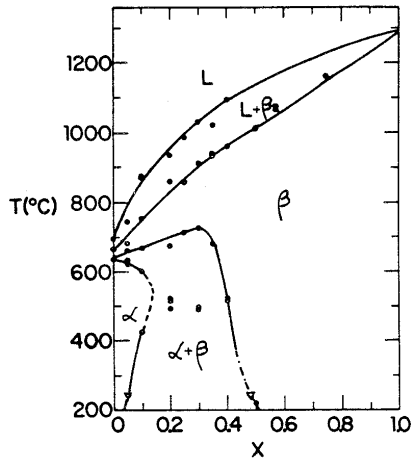

Fig. 2. $T(x)$ diagram for $Zn_{2x}(AgIn)_{1-x}Te_2$ section, (*i.e.*, $z = 0$): ∇ from x-ray data, ⊙ heating run, and ● cooling run. α is the chalcopyrite and β the zinc-blende structure.

As has been shown previously (15), $AgInTe_2$ has the chalcopyrite structure α up to 635°C and then becomes zinc-blende β up to 660°C, above which temperature it splits into a $(L + \beta_2)$ two-phase form which exists up to the liquidus at 685°C. β and β_2 are both zinc blende phases but of different composition, the β_2 phase being an In_2Te_3-rich phase in the Ag_2Te-In_2Te_3 section (15). Figures 2, 3, 4, and 5 show that in the sections $z = 0$, $x = 0$, $y = 3x$, and $x = y$, both the α and β phases are present. However, for the $x = 3y$ section (Fig. 6), the chalcopyrite phase does not occur, but a wide range of zinc blende β phases is observed. With regard to the lower temperature range, *i.e.*, mainly in the single-phase solid fields, for the $z = 0$ section (Fig. 2) it is seen that the α phase appears at 635°C for $x = 0$ and that the field achieves a maximum width of ~0.14 at

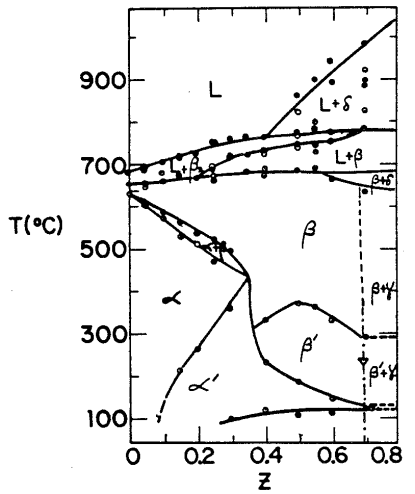

Fig. 3. $T(z)$ diagram for the $(AgIn)_{1-x}Mn_{2z}Te_2$ section, (*i.e.*, $x = 0$): ∇ from x-ray data, ⊙ heating run, and ● cooling run. α is the Mn-disordered chalcopyrite, α′ the Mn-ordered chalcopyrite, β the Mn-disordered zinc blende, β′ the Mn-ordered zinc blende, and δ and γ the NaCl and NiAs structures of MnTe, respectively.

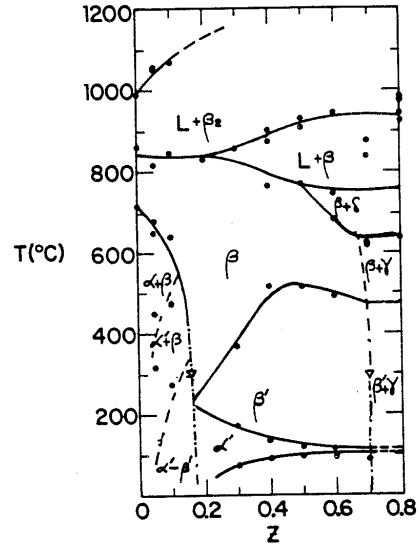

Fig. 4. $T(z)$ diagram for the $y = 3x$ section: ∇ from x-ray data, ⊙ heating run, and ● cooling run. α is the Mn-disordered chalcopyrite, α′ the Mn-ordered chalcopyrite, β the Mn-disordered zinc blende, β′ the Mn-ordered zinc blende, and δ and γ the NaCl and NiAs structures of MnTe, respectively.

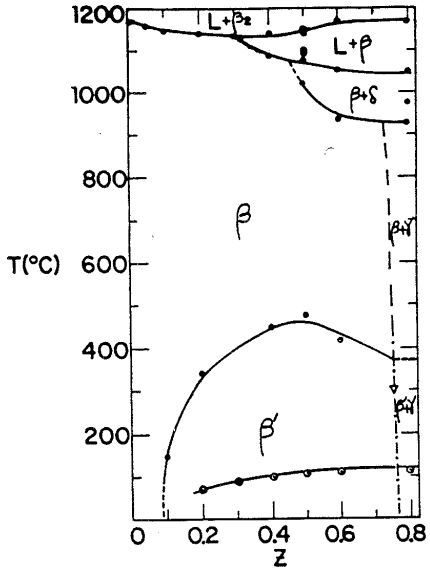

Fig. 6. $T(z)$ diagram for $x = 3y$ section: ∇ from x-ray data, ⊙ heating run, and ● cooling run. β is the Mn-disordered zinc blende, β′ the Mn-ordered zinc blende, δ and γ the NaCl and NiAs structures of MnTe, respectively.

550°C, below which temperature the range of solid solution is reduced as T is reduced. For the higher temperature range of this section, the β phase occurs at all compositions, and for $x > 0.5$ it occurs at all temperatures below the solidus curve. The α and β fields are separated by a relatively wide two-phase (α + β) field. The $x = 0$ section also shows solid solution in the α and β phases extending to $z \sim 0.7$, and for z greater than this there is a two-solid-phase field (β + γ), where γ is the NiAs structure of MnTe. The form of the (α + β) field in this section is different from that in the $z = 0$ section in that the (α + β) field is closed at low values of z, and the α-β boundary becomes a single line

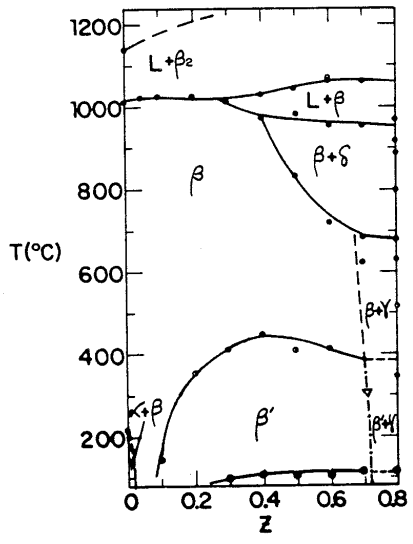

Fig. 5. $T(z)$ diagram for the $x = y$ section: ∇ from x-ray data, ⊙ heating run, and ● cooling run. α is the chalcopyrite, β the Mn-disordered zinc blende, β′ the Mn-ordered zinc blende, δ and γ the NaCl and NiAs structures of MnTe, respectively.

at the higher z values. This behavior has been attributed (5, 6) to the ordering of the Mn atoms on the cation sublattice. Ordering of manganese on this sublattice occurs for both the chalcopyrite and zinc blende structures, the ordered fields being labeled α′ and β′, respectively. Estimates based on the analysis of x-ray powder photographs for the $(AgIn)_{1-z}Mn_{2z}Te_2$ alloys (6) indicate that the manganese atoms probably lie in planes perpendicular to the c axis, the lattice showing a pseudostannite form. Measurements of magnetic susceptibility as a function of temperature on the $(CuIn)_{1-z}Mn_{2z}Te_2$ alloys (16) and on the alloys of the present $x = 0$ section (16) showed peaks corresponding to both the β′ and α′ phases over the complete range of single-phase solid solution. Re-examination of the DTA measurements for these sections showed that in addition to the transitions previously discussed (6), a β′-α′ transition is observed at lower temperatures in the range 100°-200°C, i.e., below this temperature, the chalcopyrite α′ is the equilibrium phase in the complete range of solid solution. This result is similar to that for the $(AgGa)_{1-z}Mn_{2z}Te_2$ alloys (17), where the α′ field extends to the solid solubility limit of $z = 0.55$. At still lower temperatures, around 100°C, in all of these systems a further transition is observed for $z > 0.2$, as is shown in Fig. 3-6. The phase conditions below this boundary have not as yet been determined and this will be discussed elsewhere.

The behavior of the sections $y = 3x$ and $x = y$ in this lower temperature range is very similar to that of the $x = 0$ section. However, in the $y = 3x$ section at low z values there is two-phase behavior, consistent with the form of the $z = 0$ section. Thus below 720°C, there is a (α + β) field which at lower temperatures becomes (α′ + β) and at still lower values (α′ + β′). The chalcopyrite α′ single phase occurs in the range $0.16 < z < 0.7$ at temperatures lower than 200°C, and at temperatures around 100°C, the boundary corresponding to the unknown transition mentioned above is again observed. In the case of the $x = y$ section, no single-phase α or α′ field occurs, and the (α + β) field is very narrow ($0 < z < 0.025$), occurring only below 210°C. The $x = 3y$ section differs from those discussed above in that no α or α′ phase occurs. However, as in the $x = 0$, $y = 3x$, and $x = y$ sections, there is a wide range of β field up to $z = 0.76$, while at larger z values a two-phase (β + γ) field

occurs. For both the $x = y$ and $x = 3y$ sections, the boundary corresponding to the unknown transition is observed at approximately 100°C, as is shown in Fig. 5 and 6.

At temperatures above the limit of the β field, the diagrams are more complicated and the designation of the phases in the various fields has been guided by the work of Chiang *et al.* (15) and Aresti *et al.* (5). Firstly, two different zinc-blende phases occur (15), accounting for the β_2 phase seen in the various sections. At the higher values of z, two-phase fields involving a phase δ occur, and this has been identified (5) as the rock-salt structure shown by MnTe above 1050°C but which exists at lower temperatures elsewhere in the general diagram. It is clear that, in general, none of the sections shown are pseudobinary in character. With regard to the (α + β) field, it is seen for $z = 0$ (Fig. 3) that the shape of the boundary between the β and (α + β) field indicates that the tie-lines of the (α + β) field cannot lie in the plane of the diagram, *i.e.*, the section is not pseudobinary. This is consistent with the lattice parameter and optical energy gap data obtained previously (12).

It is to be noted in Fig. 2 ($z = 0$) that peaks are observed in the range $0 < x < 0.4$ at temperatures of 500°-520°C. Similar results were found previously (17) for the $Cd_x(AgIn)_{1-x}Te_2$ alloys. This apparent solid-solid transition may be correlated with photomicrograph data on $AgInTe_2$ (18), showing the appearance of small amounts of a second phase at the grain boundaries of samples annealed at 400°C. This second phase may be associated with segregation of tellurium from the $AgInTe_2$ phase.

Conclusion

The DTA and x-ray results for the $Zn_{2x}(AgIn)_yMn_{2z}Te_2$ alloys show that a wide range of solid solution occurs for both the chalcopyrite and zinc blende structures, and that for both structures an ordered form, attributed to the Mn ions ordering on the cation sublattice, occurs below approximately 400°C for values of $z > 0.05$.

Over the whole composition range, the β phase is bounded by a two-phase ($L + \beta_2$) field. Since the β_2 phase is not represented by any point in the present composition triangle, the diagram cannot be pseudoternary nor can any pseudobinary sections be present.

Acknowledgments

The authors are grateful to Mr. G. S. Pérez and Mr. F. Sánchez for technical assistance. They wish to thank Consejo de Desarrollo Científico, Humanístico y Tecnológico (CDCHT), Universidad de Los Andes (ULA), and Consejo Nacional de Investigaciones Científicas y Tecnológicas (CONICIT) Venezuela for financial support.

Manuscript submitted June 19, 1989; revised manuscript received Jan. 25, 1990.

Universidad de Los Andes assisted in meeting the publication costs of this article.

REFERENCES

1. J. Gaj, *J. Phys. Soc. Jpn.*, **49,** 797 (1980).
2. J. K. Furdyna, *J. Appl. Phys.*, **64,** R29 (1988).
3. M. Quintero, L. Dierker, and J. C. Woolley, *J. Solid State Chem.*, **63,** 110 (1986).
4. M. Quintero and J. C. Woolley, *Phys. Status Solidi A*, **92,** 449 (1985).
5. A. Aresti, L. Garbato, A. Geddo-Lehmann, and P. Manca, Proceedings of the 7th International Conference on Ternary and Multinary Compounds, p. 497, Materials Research Society, Pittsburgh, PA (1986).
6. M. Quintero, P. Grima, R. Tovar, G. S. Pérez, and J. C. Woolley, *Phys. Status Solidi A*, **107,** 205 (1988).
7. M. Quintero, R. Tovar, M. Al-Najjar, G. Lamarche, and J. C. Woolley, *J. Solid State Chem.*, **75,** 136 (1988).
8. J. C. Woolley, G. Lamarche, A. Manoogian, M. Quintero, L. Dierker, M. Al-Najjar, D. Proulx, C. Neal, and R. Goudreault, Proceedings of the 7th International Conference on Ternary and Multinary Compounds, p. 479, Materials Research Society, Pittsburgh, PA (1986).
9. M. Quintero, P. Grima, J. E. Avon, G. Lamarche, and J. C. Woolley, *Phys. Status Solidi A*, **108,** 599 (1988).
10. M. Quintero, P. Grima, R. Tovar, R. Goudreault, D. Bissonnette, G. Lamarche, and J. C. Woolley, *J. Solid State Chem.*, **76,** 210 (1988).
11. L. Garbato and F. Ledda, *ibid.*, **30,** 189 (1979).
12. C. Neal, J. C. Woolley, R. Tovar, and M. Quintero, *J. Phys. D: Appl. Phys.*, **22,** 1347 (1989).
13. R. Tovar, M. Quintero, P. Grima, and J. C. Woolley, *Phys. Status Solidi A*, **111,** 405 (1989).
14. R. Chen and Y. Kirsh, "Analysis of Thermally Stimulated Processes," Vol. 15, p. 97, Pergamon Press, Ltd., Oxford (1981).
15. R. W. Chiang, D. F. O'Kane, and D. R. Mason, *This Journal*, **113,** 839 (1966).
16. G. Lamarche, J. C. Woolley, R. Tovar, M. Quintero, and V. Sagredo, *J. Mag. Mag. Mat.*, **80,** 321 (1989).
17. E. Guerrero, M. Quintero, and J. C. Woolley, *J. Cryst. Growth*, **92,** 150 (1988).
18. J. C. Woolley and E. W. Williams, *This Journal*, **113,** 899 (1966).